Amorphous Diamond: A High-Pressure Superhard Carbon Allotrope

Yu Lin, Li Zhang, Ho-kwang Mao, Paul Chow, Yuming Xiao, Maria Baldini, Jinfu Shu, and Wendy L. Mao

Phys. Rev. Lett. **107**, 175504 — Published 19 October 2011

DOI: 10.1103/PhysRevLett.107.175504

Amorphous diamond -- A high-pressure superhard carbon allotrope

Yu Lin[1*], Li Zhang[2], Ho-kwang Mao[2], Paul Chow[3], Yuming Xiao[3], Maria Baldini[4], Jinfu Shu[2], Wendy L. Mao[1,5]

[1]*Department of Geological and Environmental Sciences, Stanford University, Stanford, California 94305, USA.*

[2]*Geophysical Laboratory, Carnegie Institution of Washington, Washington, DC 20015, USA.*

[3]*High Pressure Collaborative Access Team, Carnegie Institution of Washington, Washington, DC 20015, USA.*

[4]*High Pressure Synergetic Consortium, Carnegie Institution of Washington, Washington, DC 20015, USA.*

[5]*Photon Science, SLAC National Accelerator Laboratory, Menlo Park, California 94025, USA.*

[*]To whom correspondence should be addressed. E-mail: lyforest@stanford.edu

Abstract

Compressing glassy carbon above 40 GPa, we have observed a new carbon allotrope with a fully sp^3-bonded amorphous structure and diamond-like strength. Synchrotron x-ray Raman spectroscopy revealed a continuous pressure-induced sp^2-to-sp^3 bonding change, while x-ray diffraction confirmed the perseverance of non-crystallinity. The transition was reversible upon releasing pressure. Used as an indentor, the glassy carbon ball demonstrated its exceptional strength by reaching 130 GPa with a confining pressure of 60 GPa. Such an extremely large stress difference of >70 GPa has never been observed in any material besides diamond, indicating the high hardness of this high-pressure carbon allotrope.

As the fourth most abundant element in the universe, carbon forms a variety of allotropes with dramatically different physical and chemical properties [1-4]. The carbon atoms in crystalline diamond are characterized by sp^3-hybridized orbitals with all four valence electrons forming tetrahedrally-coordinated σ bonds to four adjacent carbon atoms, resulting in the high density and extremely high hardness of diamond. The carbon atoms in crystalline graphite are characterized by sp^2-hybridized orbitals with three electrons forming trigonally-coordinated σ bonds to three carbon atoms in the same plane, while the fourth valence electron forms weak, long π bonds with atoms in the neighboring planes, resulting in the low density and low hardness of graphite.

Diamond, a high-pressure carbon form that is metastable at ambient conditions, possesses a myriad of attractive properties which make it a technologically important material. Decades of research has focused on the search for diamond-like materials for practical applications. High pressure serves as a clean and powerful tool which has been used to investigate a number of carbon allotropes including graphite [5-9], C_{60} and its derivatives [10-12], and carbon nanotubes [13-15]. Attractive physical/chemical/mechanical properties have been identified in these materials under compression or their high pressure modifications. For instance, the C_{60} fullerene undergoes a 1-dimensional (1D) or 2D polymerization at high pressures and/or temperatures, and further modifications into 3D network on subsequent compression with sp^3 hybridization whose hardness is comparable or even higher than that of diamond. However, these high pressure studies were based on crystalline carbon phases.

Under certain circumstances non-crystalline materials would be advantageous than crystalline forms. Extensive efforts in making diamond-like amorphous carbon [16-18] and tetrahedral amorphous carbon [19-24] using subplantation of incident ions have produced thin

films with exceptional properties of high hardness, inertness, transparency and wide-bandgap semiconductivity for applications such as protective coatings for optical, electronic, mechanical, and biomedical components. However, these carbon films have less than 88% sp^3-bonding, often contain a significant amount of hydrogenated carbon and nanocrystalline diamond, and are significantly different from a fully sp^3-bonded bulk amorphous material. In addition, high pressure amorphous carbon phases such as those obtained from fullerenes always involved shock compression [25] or pressure-temperature treatments [26, 27]. The particular pressure-temperature pathway plays a significant role in determining the final products as well as their properties, leading to controversial results reported in the literature.

Glassy carbon is an amorphous carbon allotrope, containing nearly 100% sp^2-bonding at ambient conditions. It has a fullerene-related structure [28], where fragments of curved graphene-like sheets of linked hexagons with dispersed pentagons and heptagons are randomly distributed throughout the network [29]. Glassy carbon combines desirable properties of glass and ceramics with those of graphite, such as high temperature stability, extreme resistance to chemical attack, high proportion of isolated porosity, and impermeability to gases and liquids. Here we compressed glassy carbon at ambient temperature and completely converted its sp^2-bonding to sp^3 while preserving its amorphous structure. This amorphous carbon phase also possesses diamond-like strength. Three different sets of *in-situ* high-pressure experiments were conducted. We used x-ray Raman spectroscopy (XRS) [5, 30-33] to probe the short-range carbon bonding changes, x-ray diffraction (XRD) to verify the absence of crystalline long-range order, and XRD of a potassium iodide (KI) sample compressed by a glassy carbon indenter to demonstrate its exceptional hardness above 40 GPa.

The high-pressure XRS measurements on glassy carbon up to 44.4 GPa were conducted at beamline 16-IDD of the High Pressure Collaborative Access Team (HPCAT) at the Advanced Photon Source (APS), Argonne National Laboratory (ANL). Pristine glassy carbon starting material (Alfa Aesar, glassy carbon spherical powder, type 1) was ground and loaded along with a ruby sphere as a pressure calibrant [34] into a 100 μm sample chamber in a c-BN gasket insert in a x-ray transparent beryllium gasket, and compressed between a pair of 400 μm culet diamond anvils in a panoramic diamond anvil cell (DAC). A key challenge in studying carbon K-edge XRS between two diamond anvils is to avoid signal contamination from the diamond XRS. The narrow incident x-ray beam must pass through the carbon-free gasket gap (c-BN and Be) between the two anvils without touching the anvils. The c-BN insert of 300 μm outer diameter and 100 μm thickness was used to maintain the maximum gap thickness.[35]

Incident monochromatic x-rays were focused to 50 μm horizontal x 8 μm vertical (FWHM) by a combination of a 1m-long horizontal Kirkpatrick-Baez (KB) mirror and a 200 mm-long vertical KB mirror. The DAC was oriented vertically to match the 100 μm gap between the anvils with the 8 μm width of the x-ray beam. The sample thickness was determined by scanning the sample against the 8 μm beam after each pressure increment to ensure the carbon K-edge XRS signal was only from the glassy carbon. At the highest pressure of 44.4 GPa, The sample and gasket thickness was reduced to approximately 45 μm, and this thickness was maintained along the decompression cycle. The inelastically scattered XRS signal was collected by scanning the incident x-ray energy relative to the fixed energy of 9.887 keV which was set for each of the 17-element array analyzers. The array of 2-inch diameter bent silicon (111) analyzers are close packed into 3 columns (6-5-6) in a vertical Rowland circle to focus the back scattered x-rays to a single detector (AmpTek) with the instrument energy resolution of 1.0 eV. XRS may

operate at much higher resolution which is gained at the expense of counting efficiency. For our challenging high-pressure experiment, the current 1.0 eV resolution is sufficient to resolve the carbon bonding changes. XRS signals of glassy carbon in the DAC were collected at 30° scattering angle which was optimized for counts and signal-to-noise ratio. For the scan range of 70 eV at step size of 0.5 eV, each scan took 70 min, and at least 12 scans were summed for each pressure point.

The carbon K-edge XRS spectra along the compression and decompression cycles are shown in Fig. 1. The XRS spectrum at ambient pressure (0 GPa) displays π^* and σ^* features corresponding to inter- and intra- layer features respectively of fullerene-related structure in the glassy carbon. Upon compression, the XRS spectra show an increase in the intensity of the σ^* at the expense of reducing π^* intensity. At 44.4 GPa, the π^*-component disappears, indicating the complete conversion to σ-bonds and the formation of a 100% sp^3-bonded carbon phase. The earlier observation [36] of an abrupt broadening of the glassy carbon optical Raman peak above 40 GPa can now be positively identified as the sp^2-to-sp^3 transition. Upon releasing pressure, the observation that the sp^2-bonding was gradually recovered upon decompression indicates that the bonding change at high pressure is reversible.

To investigate the amorphous structure by XRD, glassy carbon samples together with a ruby ball were loaded into the sample chamber created by drilling a 120 μm hole in a tungsten gasket in a symmetric DAC with 300 μm diamond anvils. High pressure angle dispersive XRD using a monochromatic x-ray beam (λ = 0.3982 Å) was carried out at beamline 16-IDB of HPCAT. The beam was well collimated into a size of approximately 5x7 μm^2.The background signal originating from diamond anvils was collected from the empty DAC before and after the experiment and was subtracted to get the sample XRD.

At ambient conditions, the XRD pattern of the glassy carbon clearly shows the amorphous first sharp diffraction peak (FSDP) and the second distinct peak (SDP) originated from the inter- and intra-layer distances of its fullerene-related fragments, respectively (Fig. 2). The origins of the FSDP and SDP are comparable to the (*002*) and (*100*) peaks of graphite, except that the amorphous FSDP and SDP are much broader than the corresponding crystalline peaks in graphite. Estimated from the FWHM of the FSDP and SDP at 0 GPa [37], the particle size of the sample is approximately 1 nm and 3 nm in the directions normal and parallel to the layer, respectively. Upon compression, as expected, the soft inter-layer FSDP shows very large pressure shifts while the incompressible intra-layer SDP shows minimal shifts (Fig. 2). Initially with a larger *d*-spacing than the graphite (*002)*, the FSDP compresses rapidly, and becomes similar to the (*002*) *d*-spacing of cold-compressed superhard graphite at highest pressures [5, 38] (Fig. 3). However, unlike cold-compressed graphite which remains crystalline up to the highest pressures studied and where theory proposed crystalline *M*-carbon [6, 7] and body-centered tetragonal C_4 [8, 9] polymorphs along the structural transition pathway, no crystallinity in glassy carbon was observed up to 45.4 GPa, the maximum pressure reached in this experiment. During decompression, the FSDP shifts back to the original position, confirming the reversibility of the transition.

Our XRD result is in contrast to a previous study where FSDP of glassy carbon was found to be more than twice as incompressible as the (*002)* of graphite [39]. For those energy dispersive XRD measurements, the energy dependence of the synchrotron source intensity, the efficiency of the detector, and diamond anvil absorption introduces a broad response function which is similar in width and shape to a typical amorphous XRD peak [40]. In their experiment this response function peak is centered at 3.57 Å which severely skews the FSDP of glassy

carbon towards this background peak, leading to underestimates of the shift in the FSDP position and its compressibility with pressure. In addition, the intensity drop-off of the synchrotron source and detector at high energy end leads to the absence of the SDP in their XRD pattern. Our angle dispersive XRD technique eliminates all these energy dependent problems.

By combining both the XRS and XRD results, the rehybridization of glassy carbon from sp^2 to sp^3 can be explained as the following process. Upon compression, the broken or imperfect graphitic layers progressively approach each other, accompanied by their sliding and shifting which would be promoted by the existence of large amounts of porosity in glassy carbon; simultaneously the buckling of the layers occurs due to attachment of another carbon atom to the C-C π bonds. Since the 2D structural elements in glassy carbon are initially curved, imperfect, and randomly distributed hexagonal layers, the bonding conversion is a continuous process as supported by our XRS and XRD measurements, whereas in cold-compressed graphite [5] the π^* component remained constant up to 16 GPa, then dropped to half of its original value, and remained constant at this latter value with further compression.

We further observed evidence for extraordinary hardness in this phase based on the large pressure difference generated by using a glassy carbon ball as a spherical indenter [41, 42] against diamond anvils. Glassy carbon spheres of various sizes together with a tiny ruby ball were placed in soft KI pressure transmitting medium in a sample chamber created by drilling a hole in a Re gasket, and compressed between two 400 μm culet diamond anvils (Fig. 4a). The gasket thickness was 80 μm initially. When we first placed a 70 μm glassy carbon ball in the sample chamber, it bridged between the two anvils at low pressures and was crushed before it had a chance to reach the sp^3 state. When we used a 40 μm sphere, it was not crushed with the circular outline remaining intact to the highest pressure (the larger glassy carbon sphere in Fig.

4a). This carbon ball functioned as a spherical indenter exerting pressure to the thin layer of KI caught between the ball and the diamond surface.

We used 5 μm focused x-ray beam to probe the KI XRD patterns across the glassy carbon ball from the center (indenting point) to the edge (confining region), represented by spots A and B in Fig. 4a, respectively. The pressure distribution was determined from the equation of state of KI [43]. Ruby fluorescence provided an additional, independent pressure reference. The KI pressure at the edge of the larger glassy carbon sphere, as well as the KI pressure at the center of the second smaller (25 μm) glassy carbon ball which did not bridge, was in excellent agreement with the ruby scale. We stopped at a confining pressure of 57 GPa which is near the safe limit for the 400 μm diamond anvils and is well above the pressure required for conversion to the sp^3-bonded state. The pressure difference maintained by the larger glassy carbon sphere increased rapidly with pressure (Fig. 4b). The maximum pressure generated by the glassy carbon indenter at the indention point was 127 GPa, indicating the glassy carbon ball was able to sustain a stress difference of 70 GPa. Such a large stress difference and megabar peak pressures have only been reached by diamond, but not any other material [44-47].

Having exceptional hardness in an amorphous solid can be advantageous especially if it turns out that this behavior is isotropic. In contrast, diamond's hardness is highly anisotropic. The extreme pressure-hardening behavior of this phase may be exploited as a second stage anvil or as a gasket material which hardens with pressure. This study also demonstrates the potential to characterize the structure and bonding properties of novel amorphous materials at high pressure, and that use of this element-specific probe of carbon can be extended to investigate various crystalline and amorphous carbon-bearing materials.

W. L. Mao is supported by the Department of Energy (DOE), Office of Basic Energy Sciences (BES), Division of Materials Sciences and Engineering, under contact DE-AC02-76SF00515. L. Zhang and H. Mao are supported by EFree under Grant No. DE-SC0001057. The experiments were performed at HPCAT, APS, ANL. HPCAT is supported by CIW, CDAC, UNLV and LLNL through funding from DOE-NNSA, DOE-BES and NSF. APS is supported by DOE-BES, under Contract No. DE-AC02-06CH11357. We thank W. Yang, S. Sinogeikin, Y. Ding, Y. Meng, and Y. Shi for help with the XRD experiments, and M. Guthrie for comments on XRD data interpretation. Y. Lin acknowledges support from the Stanford Graduate Fellowship and EFree for travel to APS.

[1] C. Frondel, and U. B. Marvin, Nature **214**, 587 (1967).
[2] K. S. Novoselov *et al.*, Science **306**, 666 (2004).
[3] H. W. Kroto *et al.*, Nature **318**, 162 (1985).
[4] E. D. Miller, D. C. Nesting, and J. V. Badding, Chem. Mater. **9**, 18 (1997).
[5] W. L. Mao *et al.*, Science **302**, 425 (2003).
[6] Q. Li *et al.*, Phys. Rev. Lett. **102**, 175506 (2009).
[7] Y. Liang, W. Zhang, and L. Chen, Epl **87**, 56003 (2009).
[8] K. Umemoto *et al.*, Phys. Rev. Lett. **104**, 125504 (2010).
[9] X.-F. Zhou *et al.*, Phys. Rev. B **82**, 134126 (2010).
[10] Y. Iwasa *et al.*, Science **264**, 1570 (1994).
[11] V. Blank *et al.*, Diamond Relat. Mater. **7**, 427 (1998).
[12] R. S. Kumar *et al.*, Diamond Relat. Mater. **16**, 1250 (2007).
[13] M. Popov, M. Kyotani, and Y. Koga, Diamond Relat. Mater. **12**, 833 (2003).
[14] W. L. Guo *et al.*, Phys. Rev. Lett. **93**, 245502 (2004).
[15] Z. W. Wang *et al.*, Proc. Natl. Acad. Sci. USA **101**, 13699 (2004).
[16] J. C. Angus, and C. C. Hayman, Science **241**, 913 (1988).
[17] Y. Lifshitz *et al.*, Science **297**, 1531 (2002).
[18] J. Robertson, Mat. Sci. Eng. R **37**, 129 (2002).
[19] P. H. Gaskell *et al.*, Phys. Rev. Lett. **67**, 1286 (1991).
[20] D. R. McKenzie, D. Muller, and B. A. Pailthorpe, Phys. Rev. Lett. **67**, 773 (1991).
[21] N. A. Marks *et al.*, Phys. Rev. Lett. **76**, 768 (1996).
[22] V. I. Merkulov *et al.*, Phys. Rev. Lett. **78**, 4869 (1997).
[23] C. A. Davis, G. A. J. Amaratunga, and K. M. Knowles, Phys. Rev. Lett. **80**, 3280 (1998).
[24] S. R. P. Silva *et al.*, Appl. Phys. Lett. **69**, 491 (1996).
[25] H. Hirai, and K. Kondo, Phys. Rev. B **51**, 15555 (1995).
[26] V. D. Blank *et al.*, Carbon **36**, 319 (1998).
[27] M. H. Manghnani *et al.*, Phys. Rev. B **64**, 121403 (2001).
[28] P. J. F. Harris, Phil. Mag. **84**, 3159 (2004).

[29] S. J. Townsend *et al.*, Phys. Rev. Lett. **69**, 921 (1992).
[30] J. P. Rueff *et al.*, J. Phys.: Condens. Matter **14**, 11635 (2002).
[31] Y. Meng *et al.*, Nat. Mater. **3**, 111 (2004).
[32] S. K. Lee *et al.*, Nat. Mater. **4**, 851 (2005).
[33] U. Bergmann, O. C. Mullins, and S. P. Cramer, Anal. Chem. **72**, 2609 (2000).
[34] C.-S. Zha, H. K. Mao, and R. J. Hemley, Proc. Natl. Acad. Sci. USA **97**, 13494 (2000).
[35] N. Funamori, and T. Sato, Rev. Sci. Instrum. **79**, 053903 (2008).
[36] A. F. Goncharov, High Press. Res. **8**, 607 (1991).
[37] B. E. Warren, Physical Review **59**, 693 (1941).
[38] T. Yagi *et al.*, Phys. Rev. B **46**, 6031 (1992).
[39] X. Wang *et al.*, J. Appl. Phys. **93**, 1991 (2003).
[40] L. Wang *et al.*, Appl. Phys. Lett. **91**, 103112 (2007).
[41] V. Brazhkin *et al.*, Nat. Mater. **3**, 576 (2004).
[42] Y. Zhao *et al.*, J. Mater. Res. **17**, 3139 (2002).
[43] K. Asaumi, T. Suzuki, and T. Mori, Phys. Rev. B **28**, 3529 (1983).
[44] H. K. Mao, and P. M. Bell, Science **200**, 1145 (1978).
[45] P. M. Bell, H. K. Mao, and K. Goettel, Science **226**, 542 (1984).
[46] J. A. Xu, and H. K. Mao, Science **290**, 783 (2000).
[47] L. Wang *et al.*, Proc. Natl. Acad. Sci. USA **107**, 6140 (2010).
[48] R. J. Angel, Equations of state. In Hazen, R. M., Downs, R. T. (Eds.), High-Temperature and High-Pressure Crystal Chemistry. Reviews in Mineralogy and Geochemistry, **41**, 35-60 (2001).

Figure captions

FIG. 1 (color online). High pressure XRS carbon K-edge spectra of glassy carbon collected along the compression and decompression cycles plotted as normalized scattered intensity versus energy loss (incident energy – analyzer energy). The scattered intensity is normalized to the incident energy. The lower energy peak at approximately 285 eV represents the π-bonding feature, corresponding 1*s* to π^* transition (labeled π^*), and the broad band at higher energy features the σ-bonding, corresponding 1*s* to σ^* transition (labeled σ^*). The red spectrum with 24-hour data collection time shows the complete σ-bonding in the high-pressure amorphous carbon phase. The numbers on the right side indicate pressure in GPa.

FIG. 2. XRD patterns of glassy carbon as a function of pressure up to 45.4 GPa at room temperature where the FSDP and SDP of glassy carbon are labeled at the bottom. No crystallinity was observed throughout the pressure range. The decompression pattern at 13.7 GPa indicates a reversible transition. * marks are used to denote diffraction peaks from the ruby ball, and # from the tungsten gasket. The numbers on the right side indicate pressure in GPa.

FIG. 3 (color online). The pressure dependence of the FSDP position of glassy carbon in our study compared to the (*002*) *d*-spacing of cold-compressed graphite [5, 38]. The solid blue line is the fit to the third-order Birch-Murnaghan equation of state [48] on glassy carbon. The error bars associated with the FSDP positions of glassy carbon are comparable to the size of the symbol.

FIG. 4. (a) Photomicrograph showing two glassy carbon spheres separated by a small ruby ball surrounded by soft KI medium at 20 GPa. (b) Pressure at the indenting point (spot A) of the larger glassy carbon sphere as a function of ruby fluorescence pressure. The surrounding pressure determined by the KI medium at the edge of the sample (represented by spot B) was

essentially the same as the ruby fluorescence pressure, which is illustrated by the solid line. Δ represents the pressure difference generated across the larger glassy carbon sphere in the high-pressure amorphous carbon phase.

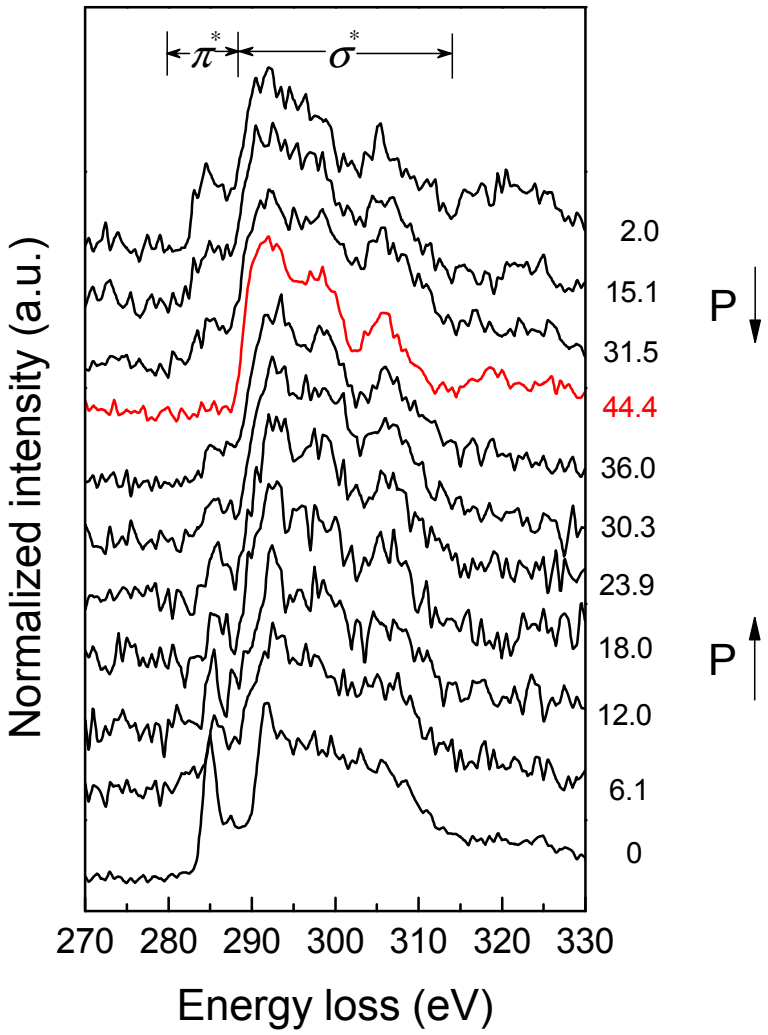
π*
σ*
2.0
15.1
31.5
44.4
36.0
30.3
23.9
18.0
12.0
6.1
0
P
P
Normalized intensity (a.u.)
270 280 290 300 310 320 330
Energy loss (eV)

FIG. 1

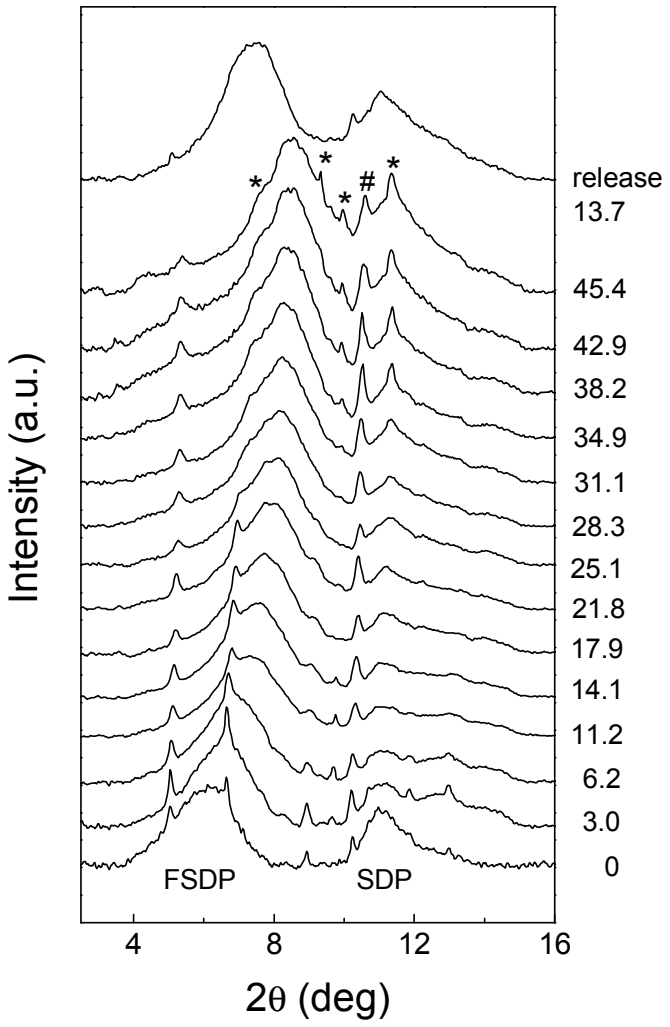
Intensity (a.u.)
release
13.7
45.4
42.9
38.2
34.9
31.1
28.3
25.1
21.8
17.9
14.1
11.2
6.2
3.0
0
FSDP
SDP
*
*
*
#
*
4
8
12
16
2θ (deg)

FIG. 2

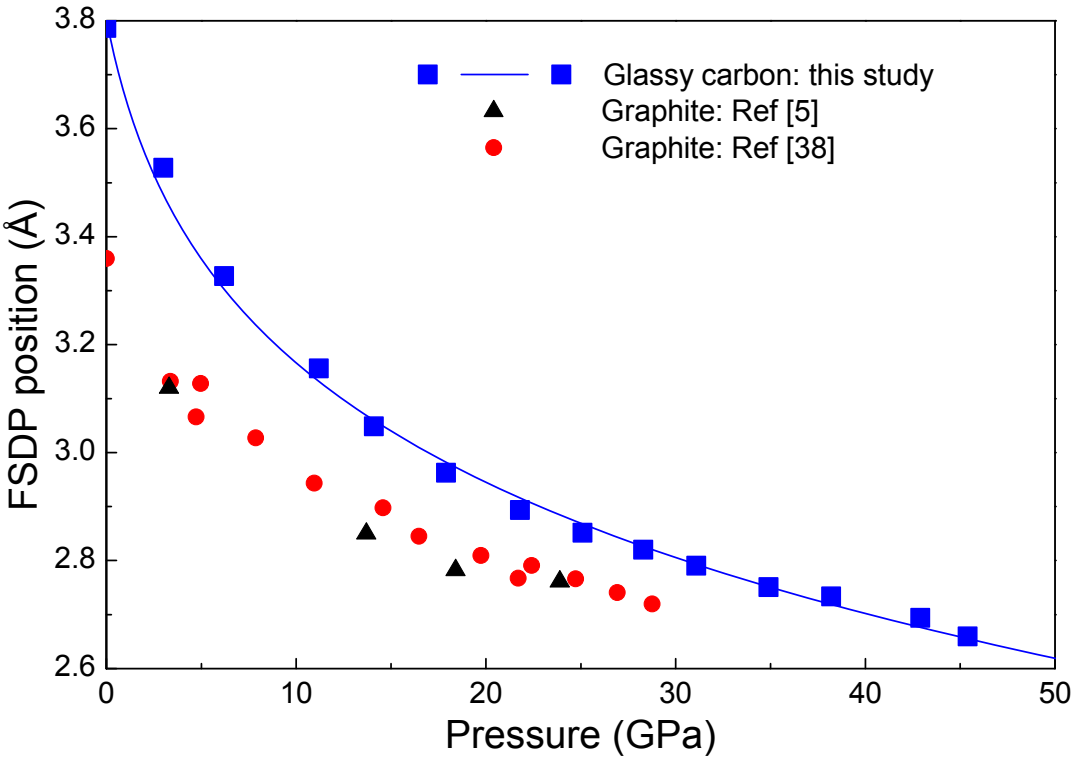
Glassy carbon: this study
Graphite: Ref [5]
Graphite: Ref [38]
FSDP position (Å)
Pressure (GPa)
3.8
3.6
3.4
3.2
3.0
2.8
2.6
0
10
20
30
40
50

FIG. 3

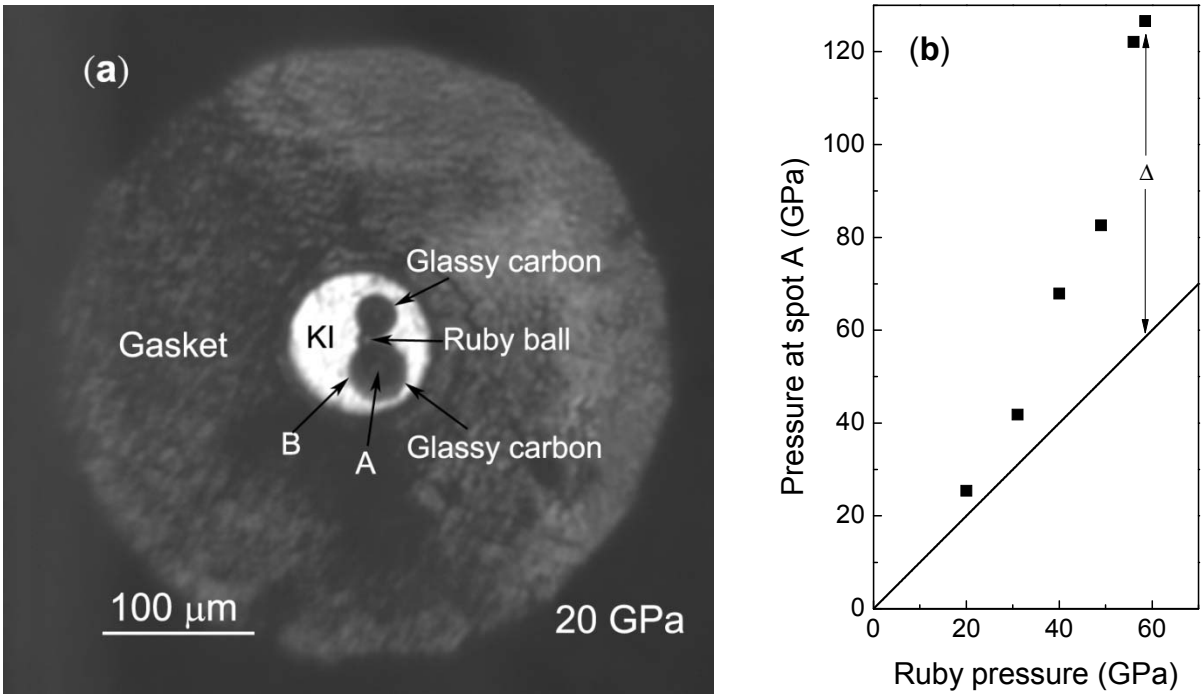
(a)
Glassy carbon
Gasket
KI
Ruby ball
B
A
Glassy carbon
100 μm
20 GPa
(b)
Δ
Pressure at spot A (GPa)
Ruby pressure (GPa)
0
20
40
60
80
100
120

FIG. 4